Ammonium CI-Orbitrap: a tool for characterizing the reactivity of oxygenated organic molecules

Dandan Li[1], Dongyu Wang[2], Lucia Caudillo[3], Wiebke Scholz[4], Mingyi Wang[5,6], Sophie Tomaz[1], Guillaume Marie[3], Mihnea Surdu[2], Elias Eccli[4], Xianda Gong[7], Loic Gonzalez-Carracedo[8], Manuel Granzin[3], Joschka Pfeifer[3,9], Birte Rörup[10], Benjamin Schulze[6], Pekka Rantala[10], Sébastien Perrier[1], Armin Hansel[4], Joachim Curtius[3], Jasper Kirkby[3,9], Neil M. Donahue[5], Christian George[1], Imad El-Haddad[2], Matthieu Riva[1,*]

[1] Univ Lyon, Université Claude Bernard Lyon 1, CNRS, IRCELYON, 69626, Villeurbanne, France

[6] Institute for Atmospheric and Earth System Research/Physics, Faculty of Science, University of Helsinki, 00014, Helsinki, Finland

[2] Laboratory of Atmospheric Chemistry, Paul Scherrer Institute, 5232, Villigen, Switzerland

[3] Institute for Atmospheric and Environmental Sciences, Goethe University Frankfurt, 60438, Frankfurt am Main, Germany

[4] Institute for Ion Physics and Applied Physics, University of Innsbruck, 6020, Innsbruck, Austria

[5] Center for Atmospheric Particle Studies, Carnegie Mellon University, Pittsburgh, PA, 15213, USA

[6] now at Division of Chemistry and Chemical Engineering, California Institute of Technology, Pasadena, CA 91125, USA

[7] Leibniz Institute for Tropospheric Research, 04318, Leipzig, Germany

[8] Faculty of Physics, University of Vienna, Vienna, 1090, Austria

[9] CERN, the European Organization for Nuclear Research, CH-1211 Geneve 23, Switzerland

[10] Institute for Atmospheric and Earth System Research/Physics, Faculty of Science, University of Helsinki, 00014, Helsinki, Finland

[*] Email: matthieu.riva@ircelyon.univ-lyon1.fr

25   Abstract

26   Oxygenated organic molecules (OOMs) play an important role in the formation of atmospheric

27   aerosols. Due to various analytical challenges in measuring organic vapors, uncertainties remain in the

28   formation and fate of OOMs. The chemical ionization Orbitrap mass spectrometer (CI-Orbitrap) has

29   recently been shown to be a powerful technique able to accurately identify gaseous organic

30   compounds due to its great mass resolving power. Here we present the ammonium ion (NH_4^+) based

31   CI-Orbitrap as a technique capable of measuring a wide range of gaseous OOMs. The performance of

32   the NH_4^+-Orbitrap was compared with that of state-of-the-art mass spectrometers, including a nitrate

33   ion (NO_3^-) based CI coupled to an atmospheric pressure interfaced to long time-of-flight mass

34   spectrometer (APi-LTOF), a new generation of proton transfer reaction-TOF mass spectrometer

35   (PTR3-TOF), and an iodide (I^-) based CI-TOF mass spectrometer equipped with a Filter Inlet for

36   Gases and AEROsols (FIGAERO-CIMS). The instruments were deployed simultaneously in the

37   Cosmic Leaving OUtdoors Droplets (CLOUD) chamber at the European Organization for Nuclear

38   Research (CERN) during the CLOUD14 campaign in 2019. Products generated from α-pinene

39   ozonolysis across multiple experimental conditions were simultaneously measured by the mass

40   spectrometers. NH_4^+-Orbitrap was able to identify the widest range of OOMs (i.e., O ≥ 2), from low

41   oxidized species to highly oxygenated organic molecules (HOMs). Excellent agreements were found

42   between the NH_4^+-Orbitrap and the NO_3^--LTOF for characterizing HOMs and with the PTR3-TOF for

43   the less oxidized monomeric species. A semi-quantitative information was retrieved for OOMs

44   measured by NH_4^+-Orbitrap using calibration factors derived from this side-by-side comparison. As

45   other mass spectrometry techniques used during this campaign, the detection sensitivity of NH_4^+-

46   Orbitrap to OOMs is greatly affected by relative humidity, which may be related to changes in

47   ionization efficiency and/or multiphase chemistry. Overall, this study shows that NH_4^+ ion-based

48   chemistry associated with the high mass resolving power of the Orbitrap mass analyzer can measure

49   almost all-inclusive compounds. As a result, it is now possible to cover the entire range of compounds,

50   which can lead to a better understanding of the oxidation processes.

51

1 Introduction

Aerosols affect the climate by either directly scattering or absorbing solar radiation, or acting as seeds for cloud formation (Fan et al., 2016; Haywood and Boucher, 2000). A major fraction of submicron aerosol mass consists of organic compounds, with secondary organic aerosol (SOA) predominating (Jimenez et al., 2009; Hallquist et al., 2009). Oxygenated organic molecules (OOMs) generated from the oxidation of volatile organic compounds (VOCs) contribute to the formation and growth of SOA (Ehn et al., 2014; Mellouki et al., 2015). OOMs can be generated through bimolecular peroxy radicals (RO_2) pathway or by the autoxidation of RO_2 followed by the termination pathways (Bianchi et al., 2019; Mohr et al., 2019). Among the OOMs, the highly oxygenated organic molecules (HOMs), containing multiple functional groups and exhibiting (extremely) low saturation vapor pressure, can nucleate in concert with inorganic species e.g., sulfuric acid or on their own (Ehn et al., 2014; Kirkby et al., 2016; Bianchi et al., 2016), forming new particles. Less oxygenated molecules (i.e., containing 2 to 5 oxygen atoms) play a vital role in the growth of newly formed atmospheric particles, either by condensation or through multiphase chemistry (Bianchi et al., 2019; Ehn et al., 2014; Hallquist et al., 2009). Therefore, the identification and quantification of the wide diversity of OOMs are essential to understand SOA formation and growth (Kirkby et al., 2016; Bianchi et al., 2016; Ehn et al., 2014).

Mass spectrometry (MS) has made remarkable achievements in detecting, characterizing, and quantifying OOMs (Wang et al., 2020; Breitenlechner et al., 2017; Bianchi et al., 2019; Ehn et al., 2010; Riva et al., 2019a). Moreover, the application of chemical ionization (CI) enables the detection of a wide variety of organic and inorganic analytes (Bianchi et al., 2019; Ehn et al., 2014; Jokinen et al., 2012; Lee et al., 2014). However, the selection of ionization chemistry in combination with MS detection technique will impact the methods selectivity and sensitivity toward certain groups of OOMs (Bianchi et al., 2019; Riva et al., 2020; Riva et al., 2019b; Berndt et al., 2018b; Berndt et al., 2018a). For example, negative ion-based chemistry, including nitrate (NO_3^-), can optimally detect HOMs, which only constitute a small subset of the OOMs (Lee et al., 2014; Berndt et al., 2018b; Riva et al., 2019b); iodide (I^-) can efficiently detect various OOMs with 3-5 oxygen atoms (Riva et al., 2019b; Lee et al., 2014). Positive ion-based chemistries have also been developed, showing great sensitivity to HOMs as well as less oxidized products, providing the possibility of achieving carbon closure of the OOMs (Berndt et al., 2018a; Berndt et al., 2018b; Hansel et al., 2018; Riva et al., 2020; Riva et al., 2019b). However, these positive ion methods are mainly based on proton transfer and often result in fragmentation of the analytes (Breitenlechner et al., 2017). Time-of-flight (TOF) mass spectrometers using ammonium (NH_4^+) or amines as reagent ions can detect a wide variety of OOMs but suffer from a lack of mass resolving power, making peak identification challenging, especially for complex systems, i.e., under ambient conditions (Berndt et al., 2018b; Berndt et al., 2018a; Riva et al., 2019b). Finally, the recently developed Orbitrap mass spectrometer using propylamine has achieved unambiguous identification of overlapping peaks and accurate quantification of OOMs (Riva et al., 2020). However, this analytical technique has been used in very diluted and dry environments to ensure a linear response to the OOMs produced from simple atmospheric systems, i.e., a single VOC precursor and oxidant (Riva et al., 2020; Riva et al., 2019b).

91　　　　Here, we explore the capability of NH_4^+ ion-based CI-Orbitrap mass spectrometer (Q-Exactive

92　　Orbitrap, Thermo Scientific) for detecting OOMs generated from α-pinene ozonolysis in the Cosmic

93　　Leaving OUtdoors Droplets (CLOUD) chamber at the European Organization for Nuclear Research

94　　(CERN) under various environmental conditions. We compare the performance of the NH_4^+-Orbitrap

95　　to state-of-the-art online mass spectrometers including a nitrate CI atmospheric pressure interface long

96　　time of flight mass spectrometer (NO_3^--LTOF; Tofwerk AG), a proton transfer reaction time of flight

97　　mass spectrometer (PTR3-TOF; Ionicon Analytik GmbH), and gas phase of an iodide CI time of flight

98　　mass spectrometer equipped with a Filter Inlet for Gases and AEROsols (I^--CIMS, Tofwerk AG).

99　　**2 Experimental approach and product analysis**

100　　**2.1 CLOUD chamber experiments**

101　　All experiments were conducted in the CLOUD chamber, a 26 m^3 cylindrical stainless-steel vessel at

102　　CERN. The chamber can achieve a pristine background for the study of nucleation (Kirkby et al.,

103　　2016). The chamber operated as a continuously stirred tank reactor (CSTR), with mixing driven by

104　　two inductively coupled fans at the top and bottom of the chamber. Evaporated liquid nitrogen (N_2)

105　　and liquid oxygen (O_2) were blended at a ratio of 79:21 to provide ultra-pure synthetic air, which

106　　flushed the chamber constantly. Variable amounts of trace gases, including O_3, VOCs, NO_x, SO_2, and

107　　CO were accurately injected into the chamber via a gas control system and monitored. Photolysis was

108　　driven by various light sources, including Hg-Xe UV lamps, and UV excimer laser. Between

109　　experiments, the chamber was cleaned by irrigating the walls with ultra-pure water, then heated to 373

110　　K, and flushed with humidified pure air and high ozone, reducing the contaminant (e.g., VOCs) to sub

111　　pptv levels. During the cleaning process, particles were removed using a high-voltage electric field.

112　　　　　The results presented here were from the CLOUD14 campaign performed in autumn 2019.

113　　During CLOUD14, the total flow was kept at 250 standard liters per minute (slpm), providing an

114　　average residence time of 104 minutes. α-Pinene was introduced into the chamber by passing a small

115　　flow of dry air over a temperature-controlled evaporator containing liquid α-pinene. Ozone was

116　　generated by flowing a small fraction of the air through a quartz tube surrounded by UVC lights

117　　(wavelength < 240 nm). Experiments were performed at low temperature (263 ± 0.1 K). The RH in the

118　　chamber was controlled by flowing a portion of the air through a Nafion® humidifier using ultrapure

119　　water (18 MΩ cm, Millipore Corporation). The contents of the chamber were monitored by a wide

120　　range of external instruments connected to the sampling probes that protrude ~1 m into the chamber.

121　　**2.2 Product analysis by NH_4^+-Orbitrap**

122　　The chemical composition of closed-shell molecules was determined in real time by means of a CI-

123　　Orbitrap sampling from the CLOUD chamber through a 750 mm long, 10 mm inner diameter Teflon

124　　tube at a flow rate of 10 slpm. The CI inlet mounted on the Orbitrap was custom-built with minor

125　　modifications from the commercial inlet (Riva et al., 2019a). The ion-molecule reaction (IMR)

126　　proceeded at atmospheric pressure with a residence time of 200-300 ms. The same operating

127　　parameters used in our previous studies (RF level 60, automatic gain control 1×10^6 charges,

128 maximum injection time 1000 ms, multi RF ratio 1.2, mass resolution m/Δm 140,000 at *m/z* 200),

129 were used, thereby minimizing declustering and maximizing the linearity range (Riva et al., 2019a;

130 Riva et al., 2020; Cai et al., 2022).

131 The high resolution Orbitrap mass spectra data were analyzed using "Orbitool" software with a

132 graphical user interface (GUI) (https://orbitrap.catalyse.cnrs.fr) (Cai et al., 2021). The analysis

133 procedures included data averaging, noise determination and reduction, single peak fitting, mass

134 calibration, assignment of molecular formulas, and export of time series. Signals were averaged over

135 5 min before determining the noise and performing mass calibration.

136 NH_4^+ has been utilized in PTR-MS with a low pressure (Berndt et al., 2018b; Hansel et al., 2018).

137 Here, this ionization technique was used to detect OOMs in atmospheric pressure and was operated in

138 a similar fashion as in our initial study (Riva et al., 2019a). NH_3 was added into the ion source by

139 flushing 2 sccm of dry air over the headspace of a 1% liquid ammonia water mixture (prepared from a

140 MilliQ water and a 25% ammonium hydroxide stock solution, ACS reagent, Sigma-Aldrich). The

141 product molecules ("prod") were softly charged by binding to ammonium (NH_4^+) ions, forming

142 (prod)-NH_4^+ adduct ions or protonated products (prod)-H^+, following either reaction (1) or (2),

143 $$NH_4^+ + prod \rightarrow (prod)\text{-}NH_4^+ \tag{1}$$

144 $$NH_4^+ + prod \rightarrow (prod\text{-}H)^+ + NH_3 \tag{2}$$
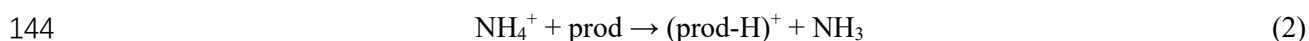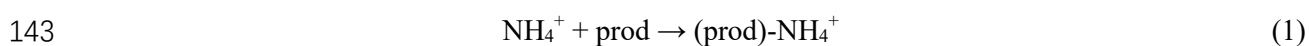
145 The NH_4^+ reagent ion cannot be directly detected due to the cut-off of the Orbitrap mass analyzer

146 (i.e, m/Q 50). Hence, normalization of the raw analyte signals is difficult and hinders quantification of

147 OOMs. However, we observed a total of 62 peaks corresponding to amines, including $C_4H_{12}N^+$, and

148 $C_6H_{14}N^+$, which are formally ammonia derivatives. To some extent, their signals can be used to

149 correct for changes in NH_4^+ ion chemistry. Among these peaks, 13 were abundant and constant

150 throughout the measurement period (Fig. S1). As a result, these signals were used as surrogates for

151 the primary reagent ions to normalize the signal intensity of the OOMs (equation 3) and to account for

152 the potential variation of the ionization process (Riva et al., 2019b).

153 $$[OOM]_{nor} = \frac{[(OOM)\text{-}NH_4^+] + [(OOM\text{-}H)^+]}{\sum[Amine]} \tag{3}$$

154 No direct calibration has been performed for the NH_4^+-Orbitrap, but a semi-quantitative method

155 was used to estimate the OOMs concentrations based on the correlation analysis using the NO_3^--

156 LTOF or the PTR3-TOF. The values of the Pearson correlation coefficients (R^2) were determined

157 between the NH_4^+-Orbitrap and two other instruments using the timeseries during two runs (run 2211

158 and 2213). This includes AP injection, steady state stage, NO_x or CO injections, and RH variation. As

159 a result, for one compound, 755 data points were recorded and used for the correlation analysis. For

160 each instrument (referred to as *REF*), OOMs with R^2 greater than 0.9 (i.e., A) between *REF* and NH_4^+-

161 Orbitrap, were used to determine a calibration factor ($c_{Orbi-REF}$, molecules cm^{-3}) and retrive the

162 concentrations of OOMs measured by the NH_4^+-Orbitrap according to the following equations 4-5:

$$c_{Orbi-REF} = \frac{[A]_{REF}}{[A]_{nor}} \qquad (4)$$

$$[OOM]_{Orbi-REF} = c_{Orbi-REF} \times [OOM]_{nor} \qquad (5)$$

The calibration factor between the NH_4^+-Orbitrap and REF (~2.62×10^8 for NO_3^--LTOF and ~4.83×10^8 for PTR3-TOF) was assumed to be constant for all the OOMs. However, decomposition of peroxides (i.e., ROOR and ROOH) can be expected within the PTR3-TOF. While fragmentation of dimeric compounds can contribute to the overall signal of the monomers, the concentration of such species remains minor (Li et al., 2022). As a result, we do not expect large enhancement of the monomers signal intensity. Finally, a temperature-dependent sampling-line loss correction factor was applied (Simon et al., 2020).

2.3 Product analysis by NO_3^--LTOF

Detection of RO_2 radicals and closed-shell products was also performed by the NO_3^--LTOF which has been described elsewhere (Jokinen et al., 2012; Caudillo et al., 2021). Therefore, only relevant details for this study are provided here. The NO_3^--LTOF used in this study had a mass resolving power of $m/\Delta m$ 12,000 and detected OOMs (mass 300-650 Da) as clusters ions with $(HNO_3)_n(NO_3^-)$ anions, with n = 0-2. The limit of detection (LoD) for OOMs is 5×10^4 molecules cm^{-3} (Simon et al., 2020). The primary ions were produced by a corona discharge needle exposed to a sheath gas enriched by HNO_3. Laminar flow diffusional loss was assumed in the 30 cm sampling line. A core-sampling technique was applied , which drew a core flow of 5.1 slpm from the center of a 30 slpm total flow. This setup reduced the sampling loss rate of HOMs to less than 30% (Simon et al., 2020).

The data were processed using Tofware (Version 3.2, Aerodyne Inc., USA) and MATLAB R2019b (MathWorks, Inc., USA). In addition, background signals, mass-dependent transmission efficiency (Heinritzi et al., 2016), and sampling losses (Simon et al., 2020) were determined and corrections were applied. The NO_3^--LTOF was directly calibrated using sulfuric acid (H_2SO_4), where the detection efficiency of HOMs was assumed as similar to H_2SO_4 . However, OOMs with less oxygen number (O < 6) were prone to a lower detection efficiency compared to H2SO4, leading to an underestimation (Stolzenburg et al., 2018; Ehn et al., 2014). A calibration factor C was determined to be ~4.13×10^{10} molecules cm^{-3} during CLOUD14 (Caudillo et al., 2021). The concentration of OOMs was also corrected using a mass dependent transmission efficiency inferred by depleting the reagent ions with several perfluorinated acids. Assuming that OOMs got lost in sampling lines due to diffusion, the losses of OOMs were corrected with a diffusion coefficient scaling with the molecular mass. More information could be found in former studies (Heinritzi et al., 2016; Stolzenburg et al., 2018; Simon et al., 2020; Caudillo et al., 2021).

2.4 Product analysis by PTR3-TOF

The PTR3-TOF ionizes organic compounds by proton transfer or ligand swith reactions where protonated water clusters $(H_2O)_nH_3O^+$ with n=1-3 were produced by a corona discharge using humidified nitrogen (Breitenlechner et al., 2017). To reduce sample losses, a 2 slpm was drawn from a

199   10 slpm laminar flow through a critical orifice into the tripole where the ion-molecule reactions occur.

200   The pressure in this region was maintained at ~80 mbar. The distribution of primary ions and sample

201   molecules can be adjusted by a tunable radio frequency signal applied to the tripole rods. The LoD of

202   PTR3-TOF for detecting OOMs is 8×10^5 molecules cm^{-3} (Breitenlechner et al., 2017).

203   During the CLOUD14 experiments, the collision energy was controlled between 62 and 72 Td to

204   reduce the methods humidity dependence which may complicate the detection of organic compounds.

205   A gas standard mixture containing 1 ppm of 3-hexanone, heptanone, and α-pinene in nitrogen was

206   dynamically diluted by a factor of 1000 in VOC-free air to contain 1 ppbv of each compound, and

207   then was used to calibrate the PTR3-TOF. All data were analyzed using TOF-Tracer software running

208   on Julia 0.6 (https://github.com/lukasfischer83/TOF-Tracer) and were further corrected for the duty

209   cycle transmission of TOF and temperature dependent sampling line losses (Stolzenburg et al., 2018).

210   On the one hand, duty cycle corrected counts per second dcps, $dcps_i = cps_i \times (101/m_i)^{1/2}$, was utilized

211   to account for the mass-dependent transmission of the TOF mass spectrometer (Breitenlechner et al.,

212   2017). The calculated sensitivities of 3-hexanone and heptanone were comparable to the observed

213   ones. Therefore, the concentration of oxygenated products was estimated using the sensitivity of 3-

214   hexanone as lower-limit values due to possible fragmentation (Breitenlechner et al., 2017;

215   Stolzenburg et al., 2018). On the other hand, the detected OOMs having (extremely) low volatility

216   were assumed to be lost by diffusion and adjusted by a temperature dependent loss-correction. The

217   sampling line losses considered three loss sections under different temperatures, including losses at

218   the sampling lines within and outside the chamber and within the PTR3-TOF instrument. Details can

219   be found in previous studies (Breitenlechner et al., 2017; Stolzenburg et al., 2018).

220   **2.5 Product analysis by I⁻-CIMS**

221   The I⁻-CIMS was capable of characterizing both gas and particle phases (Lopez-Hilfiker et al., 2014).

222   In the gas-phase mode, gases were directly sampled into a 100-mbar turbulent ion-molecule reactor,

223   while particles were collected onto a polytetrafluoroethylene (PTFE) filter through a separate

224   dedicated sampling port. Analytes were then ionized with I⁻ chemical ionization and extracted into a

225   TOF mass analyzer (Wang et al., 2020). The LoD of I⁻-CIMS for OOMs could be lower to $\sim 10^7$

226   molecules cm^{-3} (Lee et al., 2014). In this study, only gas phase data are reported.

227   Iodide ions (I⁻) were used as the reagent ions and formed by passing a 1.0 slpm flow of ultrahigh

228   purity N_2 over a diffusion tube filled with methyl iodide (CH_3I), and then through a ^{210}Po radioactive

229   source. In the sampling mode, the reagent ion flow was mixed with a sample flow in the IMR at ~150

230   mbar. Coaxial core sampling was used to minimize the vapor wall loss in the sampling line. The total

231   flow was kept at 18.0 slpm and the core flow at 4.5 slpm; the instrument sampled at the center of the

232   core flow with a flow rate of 1.6 slpm. The gas-phase background signal was determined by routinely

233   introducing zero air directly into the inlet. Data were analyzed using Tofware (2.5.11_FIGAERO

234   version; Aerodyne Inc., USA) giving 10 s average mass spectra. The ion signal was normalized by the

235   sum of reagent ion signals (i.e., m/Q 127: I⁻ and 145: H_2OI^-).

2.6 Volatility of OOMs

It is challenging to directly measure the vapor pressure of individual OOMs due to the difficulty to acquire authentic standards. To overcome experimental challenges, model calculations have been developed to estimate the vapor pressure using, for example, structure-based estimations and formula-based estimations (Pankow and Asher, 2008). Volatility basis set (VBS), a categorization framework based on quantifiable organic property (i.e., volatility) has been established and is frequently used to characterize oxidation chemistry (Donahue et al., 2011; Li et al., 2016). The VBS parameterization is useful for classifying the wide range of OOMs into multiple volatility groups, including extremely low volatility organic compounds (ELVOC) and low volatility organic compounds (LVOC) based on their effective saturation concentration (C^*) in the unit of µg m^{-3} (Bianchi et al., 2019). In this study, we applied the VBS parameterization optimized by Li et al (Li et al., 2016; Isaacman-Vanwertz and Aumont, 2021).

$$log_{10}C^*(298K) = \left(n_C^0 - n_C\right)b_C - n_O b_O - 2\frac{n_C n_O}{(n_C + n_O)}b_{CO} - n_N b_N - n_S b_S \qquad (4)$$

where n_C, n_O, n_N, and n_S was the number of carbon, oxygen, nitrogen, and sulfur atoms of the specific molecule, separately; n_C^0 was the reference carbon number; b_C, b_O, b_N, and b_S was the contribution of each atom to $log_{10}C^*$, respectively; b_{CO} was the carbon-oxygen nonideality (Donahue et al., 2011). Values of b coefficient can be found in Li et al.(Li et al., 2016). The formula used to estimate the vapor pressure was amended to convert all NO$_3$ groups into OH groups to reduce the bias from the compounds containing nitrates (Daumit et al., 2013; Isaacman-Vanwertz and Aumont, 2021).

Due to the different temperatures in the CLOUD14 experiments, we adjusted $C^*(298K)$ to the measured experimental temperature in equations (5) and (6):

$$log_{10}C^*(T) = log_{10}C^*(298K) + \frac{\Delta H_{vap}}{Rln(10)} \times \left(\frac{1}{298} - \frac{1}{T}\right) \qquad (5)$$

$$\Delta H_{vap}(kJ\ mol^{-1}) = -11 \cdot log_{10}C^*(298K) + 129 \qquad (6)$$

where T was the temperature in Kelvin, $C^*(298K)$ was the saturation vapor concentration at 298 K, ΔH_{vap} was the evaporation enthalpy and R was the gas constant (8.3134 J K^{-1} mol^{-1}). The potential presence of isomers may result in uncertainty in this method since the only input is the compound's molecular formula.

In this study, all oxidation products were grouped into six volatility regimes; ultralow-volatility (ULVOCs, C* < 10$^{-8.5}$ µg m^{-3}), extremely low volatility (ELVOCs, 10$^{-8.5}$ < C* < 10$^{-4.5}$ µg m^{-3}), low-volatility (LVOCs, 10$^{-4.5}$ < C* < 10$^{-0.5}$ µg m^{-3}), semi-volatile (SVOCs, 10$^{-0.5}$ < C* < 10$^{2.5}$ µg m^{-3}), intermediate-volatility organic compounds (IVOC, 10$^{2.5}$ < C* < 10$^{6.5}$ µg m^{-3}), and VOC (10$^{6.5}$ < C* µg m^{-3}) based on VBS.

3 Results and Discussions

3.1 Peak identification of NH_4^+-Orbitrap

As a promising reagent ion for detecting the full range of OOMs, more ions with low concentration were captured by NH_4^+, whose identification and quantification were most affected by overlapping signals. The relative intensities of neighboring peaks should also be considered when estimating their ease of separation. It has been shown that the higher mass resolution reduced the interference of adjacent peaks based on NO_3^- or $C_2H_3O_2^-$ reagent ions (Riva et al., 2019a; Riva et al., 2020). Therefore, the ability of the NH_4^+-Orbitrap for separating overlapping mass spectral peaks was compared to NH_4^+-TOF.

The mass resolving power was defined as the ratio of m to Δm, where m was the mass-to-charge ratio of the analyte ion, and Δm was the full width at half maximum (FWHM). Higher mass resolving power allows unambiguous mass spectral peak assignment. For a pair of overlapping peaks of equal intensity, the distance between their respective peak center, referred to hereafter simply as peak distance, dm, needed to be greater than approximately 0.8 of the FWHM of the overlapping peaks, such that they could be reasonably deconvolved as shown in Fig. S2. Depending on their experience, individuals may be able to visually identify the presence of overlapping peaks at lower or higher dm values. We arbitrarily defined the minimum dm (normalized to that of FWHM, or Δm) as the value at which the observed spectrum ("Combined" trace in Fig. S2 and S3) had a local minimum between the centers of the overlapping peaks (i.e., there was a "dip" in the observed signal between ion peaks). The minimum dm value increased with the intensity ratio of overlapping peaks, ranging roughly from 0.85 (for equally intense peaks) to 1.43 (for peaks differing one order of magnitude in their respective intensities), as shown in Fig. S3. In practice, noise and the presence of additional neighboring peaks would further complicate peak deconvolution. For simplicity, we used a normalized dm of 1 (i.e., $dm = \Delta m$) as a threshold for unambiguous deconvolution of neighboring peaks.

Figure 1 shows the histogram of the distances between neighboring peaks normalized against the FWHM for the NH_4^+-Orbitrap and the NH_4^+-TOF having a mass resolving power of 10,000. In each histogram, one count indicated that an ion had at least one neighboring ion with a relative intensity of 20%, 50%, or 100% (with a higher relative intensity threshold value being less selective). Neighboring ions separated by distances exceeding 2 times the FWHM were considered well-separated. For ions with multiple neighboring peaks within the 2 x FWHM separation distance window, the distance to the first neighboring peak that satisfied the aforementioned relative intensity threshold was reported. Overall, NH_4^+-Orbitrap can separate most of the observed ions (> 99%), while the NH_4^+-TOF, depending on the relative intensity threshold set, can separate only 32% to 46% of all the ions by at least 1 FWHM. It should be noted that the NH_4^+-Orbitrap has shown its strength in separating neighboring peaks in controlled experiments, in which the knowledge of the chemical compositions for OOMs is relatively abundant. The advantages of higher mass resolving power should be further stressed in ambient observations, where the knowledge about OOM species can be limited with a larger number of detectable peaks.

3.2 Characterization of OOMs by four instruments

9

307   llustrated in Fig. 2 are mass defect plots of OOMs measured by NH_4^+-Orbitrap, NO_3^--LTOF, PTR3-

308   TOF, and I^--CIMS, identifying species of 484, 252, 145, and 67, respectively in run 2211. The NH_4^+-

309   Orbitrap detected the widest range of products, including HOMs and the less oxidized species (i.e., O

310   < 6). Out of the 484 compounds, 5% were amines. The number of O atoms in OOMs varied from 1 to

311   11 in monomers (C_2-C_{10}) and from 2 to 16 for dimeric products (C_{14}-C_{20}), with an average elemental

312   oxygen-to-carbon ratio (O:C) of 0.4 ± 0.2. As expected, the NO_3^--LTOF exhibited a very good

313   sensitivity towards HOMs, with the highest O:C of 0.7 ± 0.3. The PTR3-TOF mainly detected

314   compounds below m/Q 300 Th with an average O:C of 0.5 ± 0.3, which was due to the optimization to

315   (i.e., lowering E/N value) measure ammonia and amines sensitively, which ultimately impacted its

316   capability to detect efficiently OOMs. However, many less oxygenated OOMs were still observed by

317   the PTR3-TOF and were used to conduct the correlation analysis of time series with those detected by

318   the NH_4^+-Orbitrap. Due to the selectivity and potential losses within the sampling line/inlet of the I^--

319   CIMS equipped with a FIGAERO inlet fewer monomers of C_{8-10} and dimers of C_{19-20} were observed,

320   with an average O:C of 0.5 ± 0.2.

3.3 Instrumental comparisons: correlations

322   Due to differences in selectivity and sensitivity of the analytical methods toward OOMs, ~42% of the

323   identified species by NH_4^+-Orbitrap are simultaneously detected by other mass spectrometers (Fig.

324   S4). To identify how NH_4^+-Orbitrap performed compared to the other mass spectrometers, a

325   correlation analysis including all co-detected ions was complied. The experimental conditions of the

326   runs used for performing this analysis are summarized in Table S1. The data set covered a variety of

327   conditions, such as different concentrations of α-pinene, NO_x, SO_2, and CO, as well as RH. R^2 was

328   calculated, using the time series of OOMs having the same elemental composition measured by the

329   different mass spectrometers. Figure 3 displays the correlation coefficient of time series for the

330   detected compounds, with marker size scaled by R^2. The NH_4^+-Orbitrap and the NO_3^--LTOF detected

331   OOMs with the same chemical compositions, covering monomers and dimers, among which 18

332   OOMs showed $R^2 > 0.9$. Regarding the PTR3-TOF, the NH_4^+-Orbitrap demonstrated high correlations

333   for most of the monomers and fewer dimers, including 32 species having an $R^2 > 0.9$. Due to potential

334   losses within the FIGAERO inlet, fewer OOMs were detected by the I^--CIMS. However, certain

335   families of compounds, including $C_{10}H_{15}O_{5-7}N$ and $C_{20}H_{31}O_{7,9}N$ showed high correlations (i.e., $R^2 >$

336   0.9) between the NH_4^+-Orbitrap and with the I^--CIMS. Finally, the NO_3^--LTOF was regarded as the

337   reference instrument for HOMs measurements. Only fewer monomers with high oxygen content were

338   detected by the NO_3^--LTOF and the PTR3-TOF, and only a few dimers between the NO_3^--LTOF and

339   the I^--CIMS with moderate relevance. By comparing the coverage regions of the instruments across

340   multiple experimental conditions, the NH_4^+-Orbitrap was capable of covering the widest range of

341   compounds and showed an overall good agreement with other mass spectrometers.

3.4 Instrumental comparisons: concentration estimates

343   Concentrations of the identified compounds were estimated for NH_4^+-Orbitrap, as described in section

344   2.2. The sensitivity of NH_4^+-Orbitrap was constrained using semi-quantitative information from the

345 other instruments. For instance, concentrations of the most abundant C_{10}-monomers (i.e., $C_{10}H_{14/16}O_n$)

346 were estimated using different calibration factors (Fig. 4), which were measured during steady-state

347 conditions (i.e., Run 2211 with $[O_3]$ = 100 ppbv and $[\alpha\text{-pinene}]$ = 2 ppbv, RH = 10%). The

348 concentrations of C_{10}-monomers measured by the NH_4^+-Orbitrap based on the two calibration factors

349 vary within a factor of 2, which indicates the consistency between the two correlation analyses. The

350 variation trend of concentrations with the oxygen number of the NH_4^+-Orbitrap is similar to that of the

351 NO_3^--LTOF in the range of $n_O > 6$, and it is similar to that of the PTR3-TOF in the range of $n_O = 1\sim5$.

352 Taking into consideration that such ranges are also the oxygen number ranges with high sensitivities

353 respectively, this proves the robustness of the NH_4^+-Orbitrap and the semi-quantification method. As

354 previously reported, the Orbitrap had a non-linear response to compounds present at extremely low

355 concentrations, which was independent of the sample composition, instrumental setup, or the reagent

356 ion (Riva et al., 2020; Cai et al., 2022). A similar evaluation was performed for the NH_4^+-Orbitrap by

357 comparing the measured versus the theoretical isotopic intensities. As shown in Fig. S5, the NH_4^+-

358 Orbitrap had a linear response for ion intensity greater than $\sim 5 \times 10^3$ cps, which corresponded to a

359 limit of quantification (LoQ, corresponding to the lowest normalized signal observed within the linear

360 range) of $\sim 5 \times 10^5$ molecules cm^{-3} for OOMs, estimated using the calibration factor derived from the

361 NO_3^--LTOF; which is consistent with a previous study (Riva et al., 2020).

362   Figure 5 presents the concentrations of all OOMs measured by the NH_4^+-Orbitrap determined by

363 applying two different calibration factors. The concentrations of OOMs measured by the NH_4^+-

364 Orbitrap were higher than both the NO_3^--LTOF and the PTR3-TOF which was optimized for

365 measuring ammonia and amines. This indicates that the NH_4^+-Orbitrap can provide a better constraint

366 on the concentrations of the primary products. As an example, pinonaldehyde (i.e., $C_{10}H_{16}O_2$), as one

367 of the most abundant oxidation products, was not efficiently detected by the NO_3^--LTOF, which is

368 consistent with the higher selectivity of the NO_3^- reagent ion. To further illustrate the selectivity of the

369 different reagent ions, Fig. 6 offers a summary of the performance of each mass spectrometer in

370 detecting monomeric compounds, such as $C_{10}H_{16}O_n$. The y-axis is arbitrary and represents a qualitative

371 characterization of the oxygen content when compounds were detected by different CI schemes.

372 Similar to previous results, the I^--CIMS detected OOMs with $n_O > 3$, but was not optimal for the

373 detection of monomers with $n_O > 7$ (Riva et al., 2019b). The NO_3^--LTOF was mainly selective

374 towards HOMs with $n_O > 6$ (Riva et al., 2019b). The PTR3-TOF had limited capabilities in detecting

375 OOMs with $n_O > 5$ due to the optimization of the instrument to obtain a very sensitive measurement of

376 ammonia. Previously, the amine-CI demonstrated promise for the detection of OOMs, but was limited

377 to applications with comparatively clean conditions due to considerable depletion of the reagent ion

378 and the presence of overlapping peaks (Berndt et al., 2018b; Riva et al., 2019b). While showing a

379 similar OOMs detection range to amine-CI, NH_4^+-CI in tandem with the greater mass resolving power

380 of the Orbitrap mass analyzer provided a linear response to higher loading. As shown in Fig. S6,

381 background peaks were not affected by atmospherically relevant concentrations of O_3 and α-pinene.

382 Overall, the NH_4^+-Orbitrap appears to have the potential for providing a more reliable

383   identification/quantification of OOMs produced from VOC oxidation compared to other existing mass

384   spectrometry techniques.

3.5 Volatility distribution by four instruments

386   Figure 7 shows the distribution of oxidation products measured by four MS instruments according to

387   their saturation vapor concentrations ($\log_{10}C_{sat}$) estimated using the modified Li et al. approach (Li et

388   al., 2016; Isaacman-Vanwertz and Aumont, 2021). OOMs were grouped into six volatility regimes

389   based on a volatility basis set (VBS): ultra-low volatility (ULVOCs); extremely low volatility

390   (ELVOCs); low-volatility (LVOCs); semi-volatile (SVOCs); intermediate volatility organic

391   compounds (IVOC); and VOC. ULVOCs and ELVOCs initiate cluster growth and form new particles.

392   The total signal in each volatility bin represented the sum of the signal intensity of OOMs within the

393   volatility range. The mean contributions of these compound regimes are shown in the VBS pie charts.

394   The ULVOC, ELVOC, and LVOC regimes were well captured by NH_4^+-Orbitrap and NO_3^--LTOF.

395   The PTR3-TOF only characterized the SVOC and IVOC regime (along with VOCs). IVOC and VOC

396   regimes in the PTR3-TOF and NH_4^+-Orbitrap were generally less oxygenated VOCs (i.e., $n_O < 5$).

397   IVOC comprised the biggest mass contributions for the NH_4^+-Orbitrap, and LVOC dominated in the

398   NO_3^--LTOF. Hence, the detection of the NH_4^+-Orbitrap covered the widest range of volatilities,

399   clearly highlighting the benefit of using this technique for the formation and fate of OOMs. In the past,

400   reagent switching has not been practical, and users would run multiple mass spectrometer systems in

401   parallel or use a Multi-scheme chemical IONization inlet (MION) with only one mass spectrometer to

402   obtain the fullest possible mass spectrum (Rissanen et al., 2019; Huang et al., 2021). With NH_4^+-

403   Orbitrap it is now possible to cover the entire range of compounds which was not the case with most

404   CI techniques.

3.6 RH dependance of NH_4^+-Orbitrap

406   The sensitivity of the reagent-adduct ionization has been reported to be affected by the presence of

407   water vapor for a variety of reagent ions (Lee et al., 2014; Breitenlechner et al., 2017). The impact of

408   RH on the detection of OOMs by the NH_4^+-Orbitrap was also studied. While the concentrations of gas

409   phase precursor and oxidant remained constant, the RH was raised from 10% to 80%. During this

410   increase the signal of organic vapor behaved inconsistently under an otherwise constant gas-phase

411   production rate (Surdu et al., 2023) and an increase in the condensation sink (Fig. S7). As shown in

412   Fig. 8, the NH_4^+-Orbitrap demonstrated an RH dependence. For instance, the signal of less oxygenated

413   molecules (i.e., $n_O < 5$) increased with increasing RH, especially compounds with $n_C = 8$; while the

414   signal of highly oxygenated molecules (i.e., $n_O > 10$) decreased as a function of RH. The average

415   behavior of all C_{8-10} monomers and C_{18-20} dimers was summarized and compared between four

416   instruments (Fig. S8). The other three mass spectrometers also showed obvious RH dependence.

417   Similar to NH_4^+-Orbitrap, OOMs with $n_O < 5$ measured by NO_3^--LTOF and PTR3-TOF increased at

418   high RH, and a reverse tendency for HOMs with $n_O > 11$, while OOMs with $n_O = 8\sim11$ seemed to be

419   independent to RH. The large variations of OOMs intensity at different RH measured by NH_4^+-

420   Orbitrap may be due to the widest range of oxygen atoms. The causes why OOMs with different

421 oxygen numbers measured by four instruments changed with RH was not clear. Here, multiple

422 possible reasons were provided to explain the signal evolution of the ions with changing RH, such as

423 water affecting the ionization efficiency or altering the physicochemical processes of the gas phase

424 chemistry.

425   First, the efficiency of a particular compound partly relied on whether water vapor competes with

426 the ammonium ion, lowering the sensitivity, or whether it acted as a third body to stabilize the

427 ammonium-organic analyte cluster by removing extra energy from the collision, raising the sensitivity

428 (Lee et al., 2014). NH_4^+ primary ions can cluster with water molecules when humidity increased,

429 thereby reducing the clustering of the NH_4^+ with organic analytes (Breitenlechner et al., 2017).

430 However, the formed $NH_4^+X_n$ (X being NH_3 or H_2O; n = 1,2) clusters might also act as reagent ions

431 and ionize OOMs through ligand switching reactions, which were expected to be fast and thus

432 improve the charging efficiency (Hansel et al., 2018). Compared to previous NH_4^+-CIMS, the $NH_4^+X_n$

433 reagent ions were expected to be larger due to the absence of the field in the ion-molecular-reaction

434 zone in Orbitrap, resulting in greater ligand exchanging and increasing the sensitivity for the less

435 oxygenated species (Canaval et al., 2019).

436   For RH-independent compounds, this may be due to the existence of very stable complexes with

437 NH_4^+ reagent ion, or sufficient internal vibrational modes to disperse extra energy from the collision

438 (Lee et al., 2014). The highly oxygenated dimers in the category of ULVOCs and ELVOCs which

439 largely partition to the particle phase regardless of the presence of water might indicate that water may

440 also affect the physicochemical processes (i.e., multiphase chemistry, partitioning, etc.), in this case

441 possibly leading to an increase in the driving force of gas-particle partitioning of highly oxygenated

442 species (Surdu et al., 2023), and/or causing the decomposition of highly oxygenated molecules in the

443 particle phase to create less and moderately oxygenated products, e.g., $C_8H_{12}O_{1-5}$ (up to a 30-fold

444 increase in the gas phase) (Pospisilova et al., 2020), although which in the range of SVOCs (e.g.,

445 $C_8H_{12}O_{4,5}$) was also thought to partition more to the particle phase at higher RH (Surdu et al., 2023).

446 Finally, while water vapor could affect the gas-phase chemistry through water reactions with the

447 Criegee intermediates (CIs), HO_2 chemistry, OH radical concentration, no clear evidence has been

448 identified as earlier discussed by Surdu et al (2023). However, the accurate reasons needs to be further

449 verified in target control experiments like changing the RH in IMR of CI inlet.

450 **4 Summary**

451 In conclusion, this study presented an intercomparison between NH_4^+-Orbitrap, NO_3^--LTOF, PTR3-

452 TOF, and I^--CIMS based on the identification and quantification of OOMs formed from the ozonolysis

453 of α-pinene under various environmental conditions. We used NH_4^+ adduct ions with the Orbitrap

454 mass spectrometer to measure the oxygenated species for the first time. NH_4^+-Orbitrap is a promising

455 CIMS technique for a comprehensive measurement of the whole product distribution and provides a

456 more complete understanding of the molecular composition and volatility of OOMs. This allows

457 NH_4^+-Orbitrap to better monitor the evolution of organic compounds, which can be beneficial for air

458 quality, pollutant transport, and climate models. It is worth expecting that NH_4^+-Orbitrap can be not

459 only useful for laboratory-based studies but also to field observations, to provide a deeper

460 understanding of atmospheric oxidation processes. However, it remains challenging to accurately

461 quantify the concentrations of OOMs due to the absent signals of reagent ions. In addition, RH

462 influences NH_4^+-Orbitrap sensitivity, which can be different for each OOM. Therefore, this specific

463 effect requires more attention and dedicated studies before that the NH_4^+-Orbitrap can be used in field

464 studies, for example, injection of pure or mixture of standards in atmospheric chamber at varying RH.

465 From what is presented here, the understanding of RH effect on the NH_4^+-Orbitrap capabilities is too

466 scarce to be able to understand the time series evolution of OOMs that would be obtained in the real

467 atmosphere.

Conflicts of interest

469 There are no conflicts to declare.

Author Contributions

484 D.D.L., D.Y.W., L.C., W.S., M.Y.W., S.T., G.M., M.S., E.E., X.D.G., L.G.-C., M.G., J.P., B.R., B.S.,

485 P.R., S.P., A.H., J.C., J.K., N.M.D., C.G., I.E.-H., and M.R. prepared the CLOUD facility or

486 measuring instruments. D.D.L., D.Y.W., L.C., W.S., M.Y.W., S.T., G.M., M.S., E.E., X.D.G., L.G.-

487 C., M.G., J.P., B.R., B.S., J.K., and M.R. collected the CLOUD data. D.D.L., D.Y.W., L.C., W.S.,

488 M.Y.W., G.M., and M.R.and analysed the data. D.D.L., D.Y.W., M.Y.W., N.M.D., C.G., I.E.-H., and

489 M.R. wrote the manuscript and contributed to the scientific discussion. All authors discussed the

490 results and commented on the paper.

References

492 Berndt, T., Mentler, B., Scholz, W., Fischer, L., Herrmann, H., Kulmala, M., and Hansel, A.:

493 Accretion Product Formation from Ozonolysis and OH Radical Reaction of α-Pinene: Mechanistic

494 Insight and the Influence of Isoprene and Ethylene, Environmental Science & Technology, 52, 11069-

495 11077, 10.1021/acs.est.8b02210, 2018a.

496   Berndt, T., Scholz, W., Mentler, B., Fischer, L., Herrmann, H., Kulmala, M., and Hansel, A.:

497   Accretion Product Formation from Self- and Cross-Reactions of RO$_2$ Radicals in the Atmosphere,

498   Angewandte Chemie International Edition, 57, 3820-3824, 10.1002/anie.201710989, 2018b.

499   Bianchi, F., Kurten, T., Riva, M., Mohr, C., Rissanen, M. P., Roldin, P., Berndt, T., Crounse, J. D.,

500   Wennberg, P. O., Mentel, T. F., Wildt, J., Junninen, H., Jokinen, T., Kulmala, M., Worsnop, D. R.,

501   Thornton, J. A., Donahue, N., Kjaergaard, H. G., and Ehn, M.: Highly Oxygenated Organic Molecules

502   (HOM) from Gas-Phase Autoxidation Involving Peroxy Radicals: A Key Contributor to Atmospheric

503   Aerosol, Chemical reviews, 119, 3472-3509, 10.1021/acs.chemrev.8b00395, 2019.

504   Bianchi, F., Tröstl, J., Junninen, H., Frege, C., Henne, S., Hoyle, C. R., Molteni, U., Herrmann, E.,

505   Adamov, A., Bukowiecki, N., Chen, X., Duplissy, J., Gysel, M., Hutterli, M., Kangasluoma, J.,

506   Kontkanen, J., Kürten, A., Manninen, H. E., Münch, S., Peräkylä, O., Petäjä, T., Rondo, L.,

507   Williamson, C., Weingartner, E., Curtius, J., Worsnop, D. R., Kulmala, M., Dommen, J., and

508   Baltensperger, U.: New particle formation in the free troposphere: A question of chemistry and timing,

509   Science, 352, 1109-1112, 10.1126/science.aad5456, 2016.

510   Breitenlechner, M., Fischer, L., Hainer, M., Heinritzi, M., Curtius, J., and Hansel, A.: PTR3: An

511   Instrument for Studying the Lifecycle of Reactive Organic Carbon in the Atmosphere, Analytical

512   Chemistry, 89, 5824-5831, 10.1021/acs.analchem.6b05110, 2017.

513   Cai, R., Huang, W., Meder, M., Bourgain, F., Aizikov, K., Riva, M., Bianchi, F., and Ehn, M.:

514   Improving the Sensitivity of Fourier Transform Mass Spectrometer (Orbitrap) for Online

515   Measurements of Atmospheric Vapors, Analytical chemistry, 94, 15746-15753,

516   10.1021/acs.analchem.2c03403, 2022.

517   Cai, R., Li, Y., Clément, Y., Li, D., Dubois, C., Fabre, M., Besson, L., Perrier, S., George, C., Ehn,

518   M., Huang, C., Yi, P., Ma, Y., and Riva, M.: Orbitool: a software tool for analyzing online Orbitrap

519   mass spectrometry data, Atmospheric Measurement Techniques, 14, 2377-2387, 10.5194/amt-14-

520   2377-2021, 2021.

521   Canaval, E., Hyttinen, N., Schmidbauer, B., Fischer, L., and Hansel, A.: NH$_4^+$ Association and Proton

522   Transfer Reactions With a Series of Organic Molecules, Frontiers in Chemistry, 7,

523   10.3389/fchem.2019.00191, 2019.

524   Caudillo, L., Rörup, B., Heinritzi, M., Marie, G., Simon, M., Wagner, A. C., Müller, T., Granzin, M.,

525   Amorim, A., Ataei, F., Baalbaki, R., Bertozzi, B., Brasseur, Z., Chiu, R., Chu, B., Dada, L., Duplissy,

526   J., Finkenzeller, H., Gonzalez Carracedo, L., He, X. C., Hofbauer, V., Kong, W., Lamkaddam, H.,

527   Lee, C. P., Lopez, B., Mahfouz, N. G. A., Makhmutov, V., Manninen, H. E., Marten, R., Massabò, D.,

528   Mauldin, R. L., Mentler, B., Molteni, U., Onnela, A., Pfeifer, J., Philippov, M., Piedehierro, A. A.,

529   Schervish, M., Scholz, W., Schulze, B., Shen, J., Stolzenburg, D., Stozhkov, Y., Surdu, M., Tauber,

530   C., Tham, Y. J., Tian, P., Tomé, A., Vogt, S., Wang, M., Wang, D. S., Weber, S. K., Welti, A.,

531   Yonghong, W., Yusheng, W., Zauner-Wieczorek, M., Baltensperger, U., El Haddad, I., Flagan, R. C.,

532   Hansel, A., Höhler, K., Kirkby, J., Kulmala, M., Lehtipalo, K., Möhler, O., Saathoff, H., Volkamer,

533   R., Winkler, P. M., Donahue, N. M., Kürten, A., and Curtius, J.: Chemical composition of

534   nanoparticles from α-pinene nucleation and the influence of isoprene and relative humidity at low

535   temperature, Atmospheric Chemistry and Physics, 21, 17099-17114, 10.5194/acp-21-17099-2021,

536   2021.

537   Daumit, K. E., Kessler, S. H., and Kroll, J. H.: Average chemical properties and potential formation

538   pathways of highly oxidized organic aerosol, Faraday discussions, 165, 181-202, 10.1039/c3fd00045a,

539   2013.

540   Donahue, N. M., Epstein, S. A., Pandis, S. N., and Robinson, A. L.: A two-dimensional volatility basis

541   set: 1. organic-aerosol mixing thermodynamics, Atmospheric Chemistry and Physics, 11, 3303-3318,

542   10.5194/acp-11-3303-2011, 2011.

543   Ehn, M., Junninen, H., Petäjä, T., Kurtén, T., Kerminen, V. M., Schobesberger, S., Manninen, H. E.,

544   Ortega, I. K., Vehkamäki, H., Kulmala, M., and Worsnop, D. R.: Composition and temporal behavior

545   of ambient ions in the boreal forest, Atmospheric Chemistry and Physics, 10, 8513-8530, 10.5194/acp-

546   10-8513-2010, 2010.

547   Ehn, M., Thornton, J. A., Kleist, E., Sipila, M., Junninen, H., Pullinen, I., Springer, M., Rubach, F.,

548   Tillmann, R., Lee, B., Lopez-Hilfiker, F., Andres, S., Acir, I. H., Rissanen, M., Jokinen, T.,

549   Schobesberger, S., Kangasluoma, J., Kontkanen, J., Nieminen, T., Kurten, T., Nielsen, L. B.,

550   Jorgensen, S., Kjaergaard, H. G., Canagaratna, M., Maso, M. D., Berndt, T., Petaja, T., Wahner, A.,

551   Kerminen, V. M., Kulmala, M., Worsnop, D. R., Wildt, J., and Mentel, T. F.: A large source of low-

552   volatility secondary organic aerosol, Nature, 506, 476-479, 10.1038/nature13032, 2014.

553   Fan, J., Wang, Y., Rosenfeld, D., and Liu, X.: Review of Aerosol–Cloud Interactions: Mechanisms,

554   Significance, and Challenges, Journal of the Atmospheric Sciences, 73, 4221-4252, 10.1175/jas-d-16-

555   0037.1, 2016.

556   Hallquist, M., Wenger, J. C., Baltensperger, U., Rudich, Y., Simpson, D., Claeys, M., Dommen, J.,

557   Donahue, N. M., George, C., Goldstein, A. H., Hamilton, J. F., Herrmann, H., Hoffmann, T., Iinuma,

558   Y., Jang, M., Jenkin, M. E., Jimenez, J. L., Kiendler-Scharr, A., Maenhaut, W., McFiggans, G.,

559   Mentel, T. F., Monod, A., Prévôt, A. S. H., Seinfeld, J. H., Surratt, J. D., Szmigielski, R., and Wildt,

560   J.: The formation, properties and impact of secondary organic aerosol: current and emerging issues,

561   Atmospheric Chemistry and Physics, 9, 5155-5236, 10.5194/acp-9-5155-2009, 2009.

562   Hansel, A., Scholz, W., Mentler, B., Fischer, L., and Berndt, T.: Detection of RO_2 radicals and other

563   products from cyclohexene ozonolysis with NH_4^+ and acetate chemical ionization mass spectrometry,

564   Atmospheric Environment, 186, 248-255, 10.1016/j.atmosenv.2018.04.023, 2018.

565   Haywood, J. and Boucher, O.: Estimates of the direct and indirect radiative forcing due to tropospheric

566   aerosols: A review, Reviews of Geophysics, 38, 513-543, 10.1029/1999rg000078, 2000.

Heinritzi, M., Simon, M., Steiner, G., Wagner, A. C., Kürten, A., Hansel, A., and Curtius, J.: Characterization of the mass-dependent transmission efficiency of a CIMS, Atmospheric Measurement Techniques, 9, 1449-1460, 10.5194/amt-9-1449-2016, 2016.

Huang, W., Li, H., Sarnela, N., Heikkinen, L., Tham, Y. J., Mikkilä, J., Thomas, S. J., Donahue, N. M., Kulmala, M., and Bianchi, F.: Measurement report: Molecular composition and volatility of gaseous organic compounds in a boreal forest – from volatile organic compounds to highly oxygenated organic molecules, Atmospheric Chemistry and Physics, 21, 8961-8977, 10.5194/acp-21-8961-2021, 2021.

Isaacman-VanWertz, G. and Aumont, B.: Impact of organic molecular structure on the estimation of atmospherically relevant physicochemical parameters, Atmospheric Chemistry and Physics, 21, 6541-6563, 10.5194/acp-21-6541-2021, 2021.

Jimenez, J. L., Canagaratna, M. R., Donahue, N. M., Prevot, A. S. H., Zhang, Q., Kroll, J. H., DeCarlo, P. F., Allan, J. D., Coe, H., Ng, N. L., Aiken, A. C., Docherty, K. S., Ulbrich, I. M., Grieshop, A. P., Robinson, A. L., Duplissy, J., Smith, J. D., Wilson, K. R., Lanz, V. A., Hueglin, C., Sun, Y. L., Tian, J., Laaksonen, A., Raatikainen, T., Rautiainen, J., Vaattovaara, P., Ehn, M., Kulmala, M., Tomlinson, J. M., Collins, D. R., Cubison, M. J., Dunlea, J., Huffman, J. A., Onasch, T. B., Alfarra, M. R., Williams, P. I., Bower, K., Kondo, Y., Schneider, J., Drewnick, F., Borrmann, S., Weimer, S., Demerjian, K., Salcedo, D., Cottrell, L., Griffin, R., Takami, A., Miyoshi, T., Hatakeyama, S., Shimono, A., Sun, J. Y., Zhang, Y. M., Dzepina, K., Kimmel, J. R., Sueper, D., Jayne, J. T., Herndon, S. C., Trimborn, A. M., Williams, L. R., Wood, E. C., Middlebrook, A. M., Kolb, C. E., Baltensperger, U., and Worsnop, D. R.: Evolution of Organic Aerosols in the Atmosphere, Science, 326, 1525-1529, doi:10.1126/science.1180353, 2009.

Jokinen, T., Sipilä, M., Junninen, H., Ehn, M., Lönn, G., Hakala, J., Petäjä, T., Mauldin, R. L., Kulmala, M., and Worsnop, D. R.: Atmospheric sulphuric acid and neutral cluster measurements using CI-APi-TOF, Atmospheric Chemistry and Physics, 12, 4117-4125, 10.5194/acp-12-4117-2012, 2012.

Kirkby, J., Duplissy, J., Sengupta, K., Frege, C., Gordon, H., Williamson, C., Heinritzi, M., Simon, M., Yan, C., Almeida, J., Tröstl, J., Nieminen, T., Ortega, I. K., Wagner, R., Adamov, A., Amorim, A., Bernhammer, A.-K., Bianchi, F., Breitenlechner, M., Brilke, S., Chen, X., Craven, J., Dias, A., Ehrhart, S., Flagan, R. C., Franchin, A., Fuchs, C., Guida, R., Hakala, J., Hoyle, C. R., Jokinen, T., Junninen, H., Kangasluoma, J., Kim, J., Krapf, M., Kürten, A., Laaksonen, A., Lehtipalo, K., Makhmutov, V., Mathot, S., Molteni, U., Onnela, A., Peräkylä, O., Piel, F., Petäjä, T., Praplan, A. P., Pringle, K., Rap, A., Richards, N. A. D., Riipinen, I., Rissanen, M. P., Rondo, L., Sarnela, N., Schobesberger, S., Scott, C. E., Seinfeld, J. H., Sipilä, M., Steiner, G., Stozhkov, Y., Stratmann, F., Tomé, A., Virtanen, A., Vogel, A. L., Wagner, A. C., Wagner, P. E., Weingartner, E., Wimmer, D., Winkler, P. M., Ye, P., Zhang, X., Hansel, A., Dommen, J., Donahue, N. M., Worsnop, D. R., Baltensperger, U., Kulmala, M., Carslaw, K. S., and Curtius, J.: Ion-induced nucleation of pure biogenic particles, Nature, 533, 521, 10.1038/nature17953, 2016.

Lee, B. H., Lopez-Hilfiker, F. D., Mohr, C., Kurtén, T., Worsnop, D. R., and Thornton, J. A.: An Iodide-Adduct High-Resolution Time-of-Flight Chemical-Ionization Mass Spectrometer: Application to Atmospheric Inorganic and Organic Compounds, Environmental Science & Technology, 48, 6309-6317, 10.1021/es500362a, 2014.

Li, H., Almeida, T. G., Luo, Y., Zhao, J., Palm, B. B., Daub, C. D., Huang, W., Mohr, C., Krechmer, J. E., Kurtén, T., and Ehn, M.: Fragmentation inside proton-transfer-reaction-based mass spectrometers limits the detection of ROOR and ROOH peroxides, Atmospheric Measurement Techniques, 15, 1811-1827, 10.5194/amt-15-1811-2022, 2022.

Li, Y., Pöschl, U., and Shiraiwa, M.: Molecular corridors and parameterizations of volatility in the chemical evolution of organic aerosols, Atmospheric Chemistry and Physics, 16, 3327-3344, 10.5194/acp-16-3327-2016, 2016.

Lopez-Hilfiker, F. D., Mohr, C., Ehn, M., Rubach, F., Kleist, E., Wildt, J., Mentel, T. F., Lutz, A., Hallquist, M., Worsnop, D., and Thornton, J. A.: A novel method for online analysis of gas and particle composition: description and evaluation of a Filter Inlet for Gases and AEROsols (FIGAERO), Atmospheric Measurement Techniques, 7, 983-1001, 10.5194/amt-7-983-2014, 2014.

Mellouki, A., Wallington, T. J., and Chen, J.: Atmospheric chemistry of oxygenated volatile organic compounds: impacts on air quality and climate, Chemical reviews, 115, 3984-4014, 10.1021/cr500549n, 2015.

Mohr, C., Thornton, J. A., Heitto, A., Lopez-Hilfiker, F. D., Lutz, A., Riipinen, I., Hong, J., Donahue, N. M., Hallquist, M., Petäjä, T., Kulmala, M., and Yli-Juuti, T.: Molecular identification of organic vapors driving atmospheric nanoparticle growth, Nature Communications, 10, 10.1038/s41467-019-12473-2, 2019.

Pospisilova, V., Lopez-Hilfiker, F. D., Bell, D. M., El Haddad, I., Mohr, C., Huang, W., Heikkinen, L., Xiao, M., Dommen, J., Prevot, A. S. H., Baltensperger, U., and Slowik, J. G.: On the fate of oxygenated organic molecules in atmospheric aerosol particles, Science Advances, 6, eaax8922, doi:10.1126/sciadv.aax8922, 2020.

Rissanen, M. P., Mikkilä, J., Iyer, S., and Hakala, J.: Multi-scheme chemical ionization inlet (MION) for fast switching of reagent ion chemistry in atmospheric pressure chemical ionization mass spectrometry (CIMS) applications, Atmospheric Measurement Techniques, 12, 6635-6646, 10.5194/amt-12-6635-2019, 2019.

Riva, M., Brüggemann, M., Li, D., Perrier, S., George, C., Herrmann, H., and Berndt, T.: Capability of CI-Orbitrap for Gas-Phase Analysis in Atmospheric Chemistry: A Comparison with the CI-APi-TOF Technique, Analytical Chemistry, 92, 8142-8150, 10.1021/acs.analchem.0c00111, 2020.

Riva, M., Ehn, M., Li, D., Tomaz, S., Bourgain, F., Perrier, S., and George, C.: CI-Orbitrap: An Analytical Instrument To Study Atmospheric Reactive Organic Species, Analytical Chemistry, 91, 9419-9423, 10.1021/acs.analchem.9b02093, 2019a.

640   Riva, M., Rantala, P., Krechmer, J. E., Peräkylä, O., Zhang, Y., Heikkinen, L., Garmash, O., Yan, C.,
641   Kulmala, M., Worsnop, D., and Ehn, M.: Evaluating the performance of five different chemical
642   ionization techniques for detecting gaseous oxygenated organic species, Atmospheric Measurement
643   Techniques, 12, 2403-2421, 10.5194/amt-12-2403-2019, 2019b.

644   Schobesberger, S., Junninen, H., Bianchi, F., Lonn, G., Ehn, M., Lehtipalo, K., Dommen, J., Ehrhart,
645   S., Ortega, I. K., Franchin, A., Nieminen, T., Riccobono, F., Hutterli, M., Duplissy, J., Almeida, J.,
646   Amorim, A., Breitenlechner, M., Downard, A. J., Dunne, E. M., Flagan, R. C., Kajos, M., Keskinen,
647   H., Kirkby, J., Kupc, A., Kurten, A., Kurten, T., Laaksonen, A., Mathot, S., Onnela, A., Praplan, A. P.,
648   Rondo, L., Santos, F. D., Schallhart, S., Schnitzhofer, R., Sipila, M., Tome, A., Tsagkogeorgas, G.,
649   Vehkamaki, H., Wimmer, D., Baltensperger, U., Carslaw, K. S., Curtius, J., Hansel, A., Petaja, T.,
650   Kulmala, M., Donahue, N. M., and Worsnop, D. R.: Molecular understanding of atmospheric particle
651   formation from sulfuric acid and large oxidized organic molecules, Proceedings of the National
652   Academy of Sciences of the United States of America, 110, 17223-17228, 10.1073/pnas.1306973110,
653   2013.

654   Simon, M., Dada, L., Heinritzi, M., Scholz, W., Stolzenburg, D., Fischer, L., Wagner, A. C., Kürten,
655   A., Rörup, B., He, X.-C., Almeida, J., Baalbaki, R., Baccarini, A., Bauer, P. S., Beck, L., Bergen, A.,
656   Bianchi, F., Bräkling, S., Brilke, S., Caudillo, L., Chen, D., Chu, B., Dias, A., Draper, D. C., Duplissy,
657   J., El-Haddad, I., Finkenzeller, H., Frege, C., Gonzalez-Carracedo, L., Gordon, H., Granzin, M.,
658   Hakala, J., Hofbauer, V., Hoyle, C. R., Kim, C., Kong, W., Lamkaddam, H., Lee, C. P., Lehtipalo, K.,
659   Leiminger, M., Mai, H., Manninen, H. E., Marie, G., Marten, R., Mentler, B., Molteni, U., Nichman,
660   L., Nie, W., Ojdanic, A., Onnela, A., Partoll, E., Petäjä, T., Pfeifer, J., Philippov, M., Quéléver, L. L.
661   J., Ranjithkumar, A., Rissanen, M. P., Schallhart, S., Schobesberger, S., Schuchmann, S., Shen, J.,
662   Sipilä, M., Steiner, G., Stozhkov, Y., Tauber, C., Tham, Y. J., Tomé, A. R., Vazquez-Pufleau, M.,
663   Vogel, A. L., Wagner, R., Wang, M., Wang, D. S., Wang, Y., Weber, S. K., Wu, Y., Xiao, M., Yan,
664   C., Ye, P., Ye, Q., Zauner-Wieczorek, M., Zhou, X., Baltensperger, U., Dommen, J., Flagan, R. C.,
665   Hansel, A., Kulmala, M., Volkamer, R., Winkler, P. M., Worsnop, D. R., Donahue, N. M., Kirkby, J.,
666   and Curtius, J.: Molecular understanding of new-particle formation from α-pinene between −50 and
667   +25 °C, Atmospheric Chemistry and Physics, 20, 9183-9207, 10.5194/acp-20-9183-2020, 2020.

668   Stolzenburg, D., Fischer, L., Vogel, A. L., Heinritzi, M., Schervish, M., Simon, M., Wagner, A. C.,
669   Dada, L., Ahonen, L. R., Amorim, A., Baccarini, A., Bauer, P. S., Baumgartner, B., Bergen, A.,
670   Bianchi, F., Breitenlechner, M., Brilke, S., Buenrostro Mazon, S., Chen, D., Dias, A., Draper, D. C.,
671   Duplissy, J., El Haddad, I., Finkenzeller, H., Frege, C., Fuchs, C., Garmash, O., Gordon, H., He, X.,
672   Helm, J., Hofbauer, V., Hoyle, C. R., Kim, C., Kirkby, J., Kontkanen, J., Kürten, A., Lampilahti, J.,
673   Lawler, M., Lehtipalo, K., Leiminger, M., Mai, H., Mathot, S., Mentler, B., Molteni, U., Nie, W.,
674   Nieminen, T., Nowak, J. B., Ojdanic, A., Onnela, A., Passananti, M., Petäjä, T., Quéléver, L. L. J.,
675   Rissanen, M. P., Sarnela, N., Schallhart, S., Tauber, C., Tomé, A., Wagner, R., Wang, M., Weitz, L.,
676   Wimmer, D., Xiao, M., Yan, C., Ye, P., Zha, Q., Baltensperger, U., Curtius, J., Dommen, J., Flagan,
677   R. C., Kulmala, M., Smith, J. N., Worsnop, D. R., Hansel, A., Donahue, N. M., and Winkler, P. M.:
678   Rapid growth of organic aerosol nanoparticles over a wide tropospheric temperature range,
679   Proceedings of the National Academy of Sciences, 115, 9122-9127, 10.1073/pnas.1807604115, 2018.

19

680   Surdu, M., Lamkaddam, H., Wang, D. S., Bell, D. M., Xiao, M., Lee, C. P., Li, D., Caudillo, L.,
681   Marie, G., Scholz, W., Wang, M., Lopez, B., Piedehierro, A. A., Ataei, F., Baalbaki, R., Bertozzi, B.,
682   Bogert, P., Brasseur, Z., Dada, L., Duplissy, J., Finkenzeller, H., He, X.-C., Höhler, K., Korhonen, K.,
683   Krechmer, J. E., Lehtipalo, K., Mahfouz, N. G. A., Manninen, H. E., Marten, R., Massabò, D.,
684   Mauldin, R., Petäjä, T., Pfeifer, J., Philippov, M., Rörup, B., Simon, M., Shen, J., Umo, N. S., Vogel,
685   F., Weber, S. K., Zauner-Wieczorek, M., Volkamer, R., Saathoff, H., Möhler, O., Kirkby, J., Worsnop,
686   D. R., Kulmala, M., Stratmann, F., Hansel, A., Curtius, J., Welti, A., Riva, M., Donahue, N. M.,
687   Baltensperger, U., and El Haddad, I.: Molecular Understanding of the Enhancement in Organic
688   Aerosol Mass at High Relative Humidity, Environmental Science & Technology, 57, 2297-2309,
689   10.1021/acs.est.2c04587, 2023.

690   Wang, M., Kong, W., Marten, R., He, X.-C., Chen, D., Pfeifer, J., Heitto, A., Kontkanen, J., Dada, L.,
691   Kürten, A., Yli-Juuti, T., Manninen, H. E., Amanatidis, S., Amorim, A., Baalbaki, R., Baccarini, A.,
692   Bell, D. M., Bertozzi, B., Bräkling, S., Brilke, S., Murillo, L. C., Chiu, R., Chu, B., De Menezes, L.-P.,
693   Duplissy, J., Finkenzeller, H., Carracedo, L. G., Granzin, M., Guida, R., Hansel, A., Hofbauer, V.,
694   Krechmer, J., Lehtipalo, K., Lamkaddam, H., Lampimäki, M., Lee, C. P., Makhmutov, V., Marie, G.,
695   Mathot, S., Mauldin, R. L., Mentler, B., Müller, T., Onnela, A., Partoll, E., Petäjä, T., Philippov, M.,
696   Pospisilova, V., Ranjithkumar, A., Rissanen, M., Rörup, B., Scholz, W., Shen, J., Simon, M., Sipilä,
697   M., Steiner, G., Stolzenburg, D., Tham, Y. J., Tomé, A., Wagner, A. C., Wang, D. S., Wang, Y.,
698   Weber, S. K., Winkler, P. M., Wlasits, P. J., Wu, Y., Xiao, M., Ye, Q., Zauner-Wieczorek, M., Zhou,
699   X., Volkamer, R., Riipinen, I., Dommen, J., Curtius, J., Baltensperger, U., Kulmala, M., Worsnop, D.
700   R., Kirkby, J., Seinfeld, J. H., El-Haddad, I., Flagan, R. C., and Donahue, N. M.: Rapid growth of new
701   atmospheric particles by nitric acid and ammonia condensation, Nature, 581, 184-189,
702   10.1038/s41586-020-2270-4, 2020.

703

704
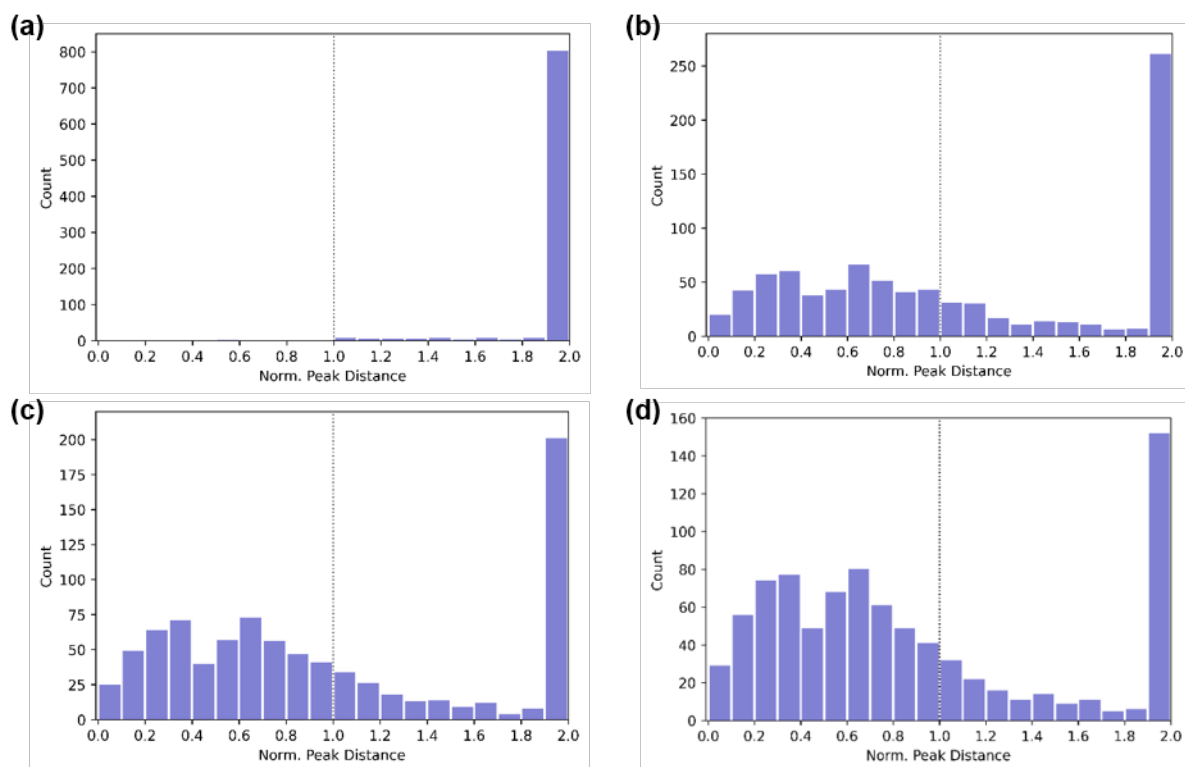
Figure 1: Number of adjacent peaks within a intensity threshold as the function of normalized peak distance observed by (a) NH_4^+-Orbitrap and (b, c, d) NH_4^+-TOF, respectively. The normalized peak distance was the ratio of distance between neighboring peaks to the full width at half maximum (FWHM). For each ion, the distance to the closest neighbor with a relative peak intensity that exceeded 20%, 50%, or 100% is recorded. (a) Orbitrap mass analyzer >99% of ions were separated by at least 1 FWHM from their neighbors with relative intensity threshold being set at 20%. (b) TOF mass analyzer (mass resolution ~10,000) >46% of ions were separated by at least 1 FWHM from their neighbors with a relative intensity threshold being set at 100%. (c) TOF mass analyzer >39% of ions were separated by at least 1 FWHM from their neighbors with a relative intensity threshold being set at 50%. (d) TOF mass analyzer >32% of ions were separated by at least 1 FWHM from their neighbors with a relative intensity threshold being set at 20%.
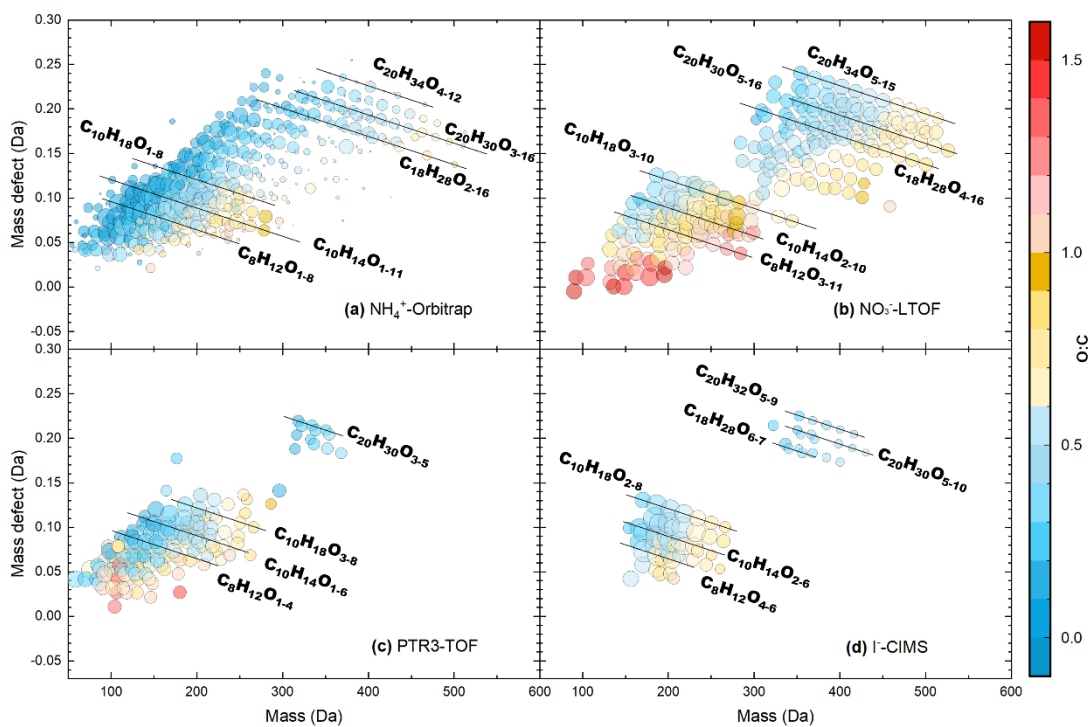
Figure 2: Mass defect plots for organic compounds measured by (a) NH_4^+-Orbitrap, (b) NO_3^--LTOF, (c) PTR3-TOF and (d) I^--CIMS in run 2211. The x-axis represents the mass-to-charge ratio of the neutral analyte and the y-axis represents the corresponding mass defect, which is the difference between their exact mass and nominal mass (Schobesberger et al., 2013). Markers were all sized by the logarithm of their corresponding signals and colored by the O:C value. Some major OOMs measured by different instruments were indicated by the black lines.

22
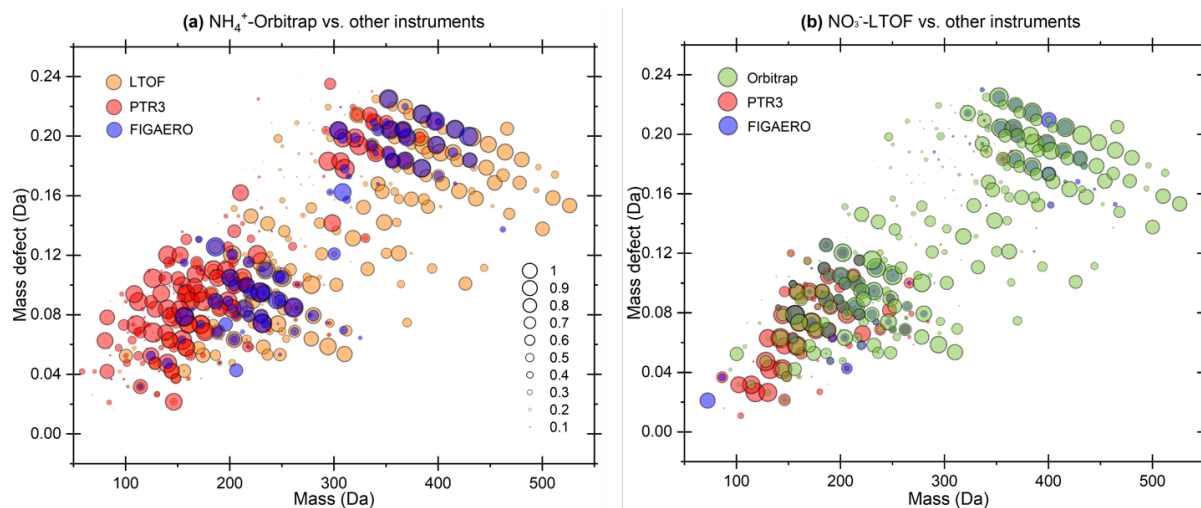
Figure 3: Mass defect plots depicting the compounds of which time series correlation was observed by (a) NH_4^+-Orbitrap and (b) NO_3^--LTOF with other MS instruments. Each circle represents a molecule and marker size represents the correlation R^2 of time series of the molecules between two different MS instruments. Two sets of data in run 2211 and 2213 were used to reduce uncertainties.
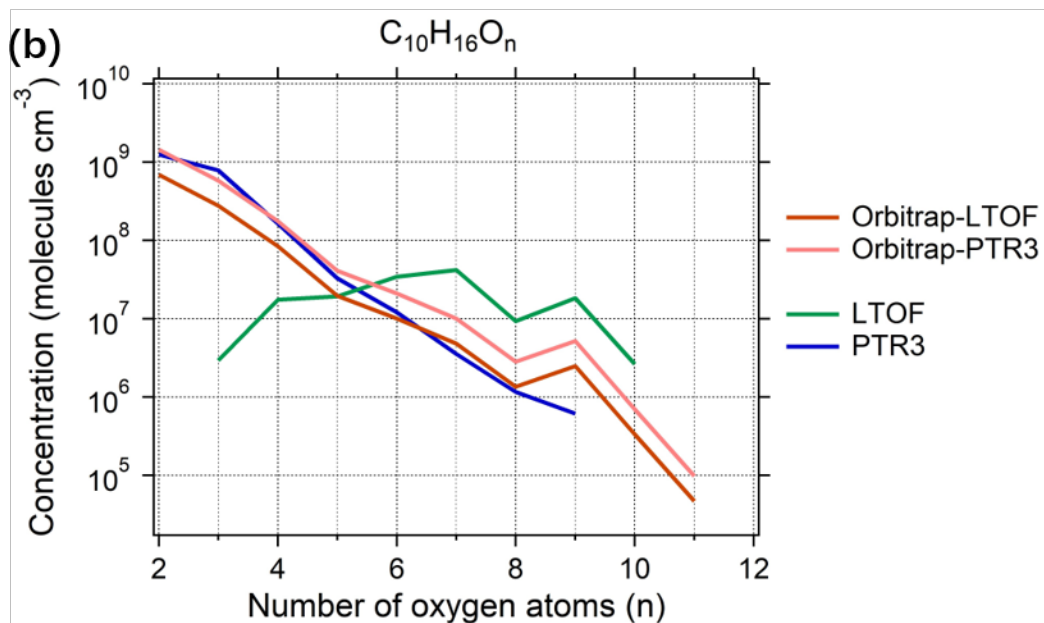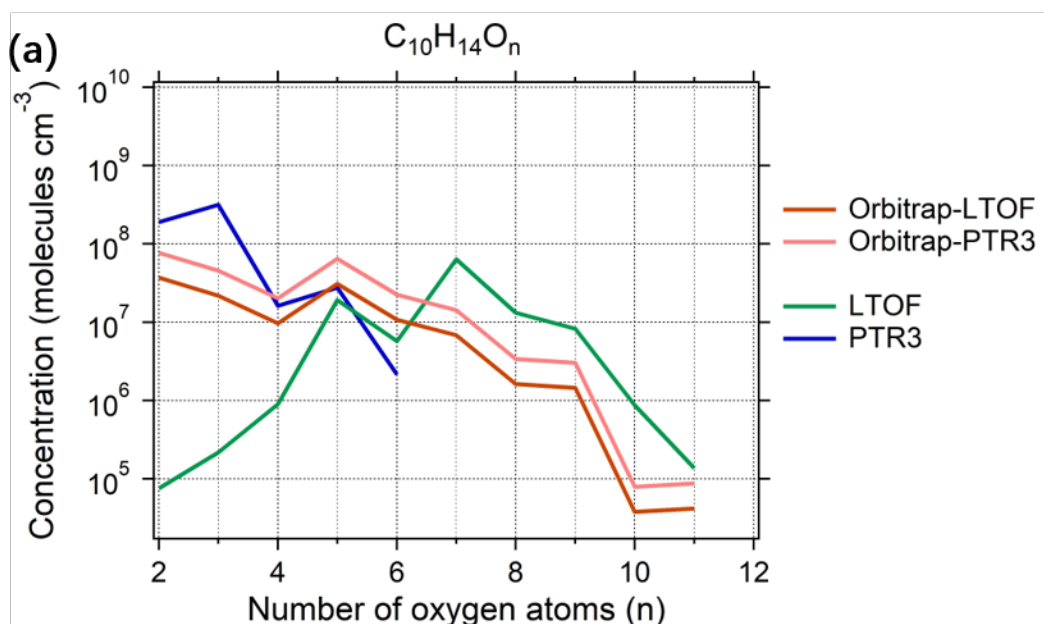
Figure 4: Estimated concentrations of the main C_{10} oxidation products (a) $C_{10}H_{14}O_n$ and (b) $C_{10}H_{16}O_n$ as a function of oxygen numbers observed in run 2211. Orbitrap-LTOF and Orbitrap-PTR3 represented the estimated concentration of monomers measured by NH_4^+-Orbitrap using the calibration factors from the correlation analysis with NO_3^--LTOF and PTR3-TOF, respectively.

733
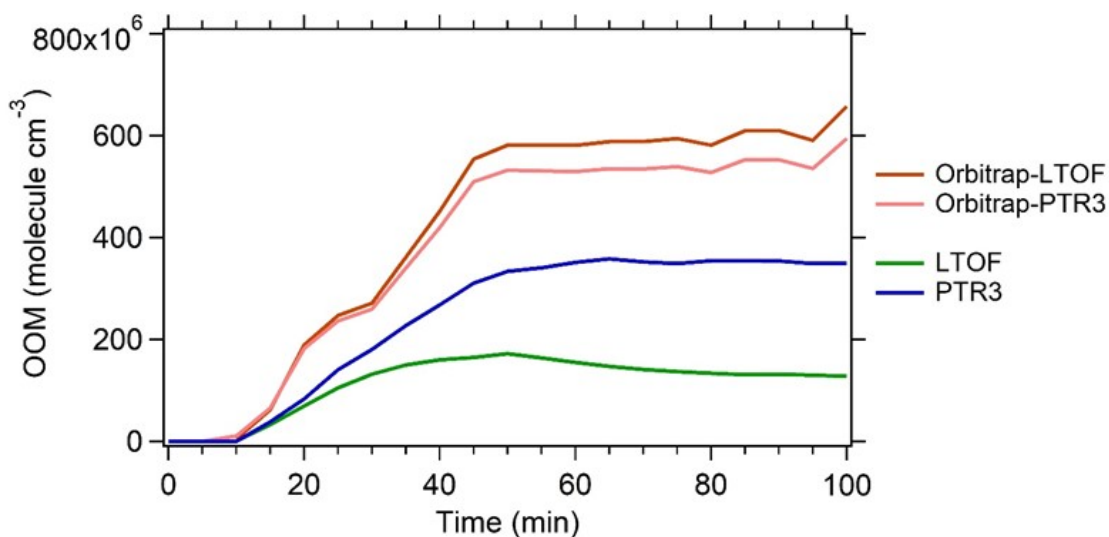
Figure 5: Estimated concentrations of all measured OOMs in the photooxidation of α-pinene. All
monomers C_{8-10} and dimers C_{18-20} measured by NH_4^+-Orbitrap, NO_3^--LTOF, and PTR3-TOF in run
2213 were summed up. The concentrations of OOMs measured by NH_4^+-Orbitrap were quantified by
the calibration factors derived from correlation analysis between NH_4^+-Orbitrap and NO_3^--LTOF
(Orbitrap-LTOF, light green) or PTR3-TOF (Orbitrap-PTR3, light blue), respectively.
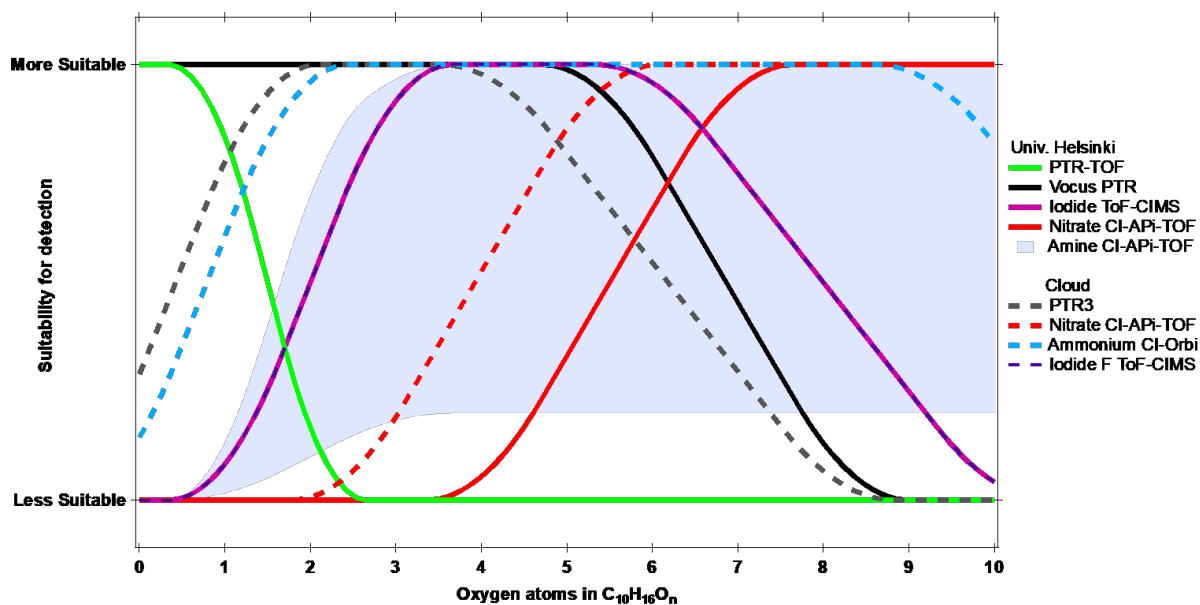
**Figure 6:** Estimated detection suitability of the different CIMS techniques for monomers from α-pinene ozonolysis, plotted as a function of the number of oxygen atoms. Image modified from Riva et al.(Riva et al., 2019b).
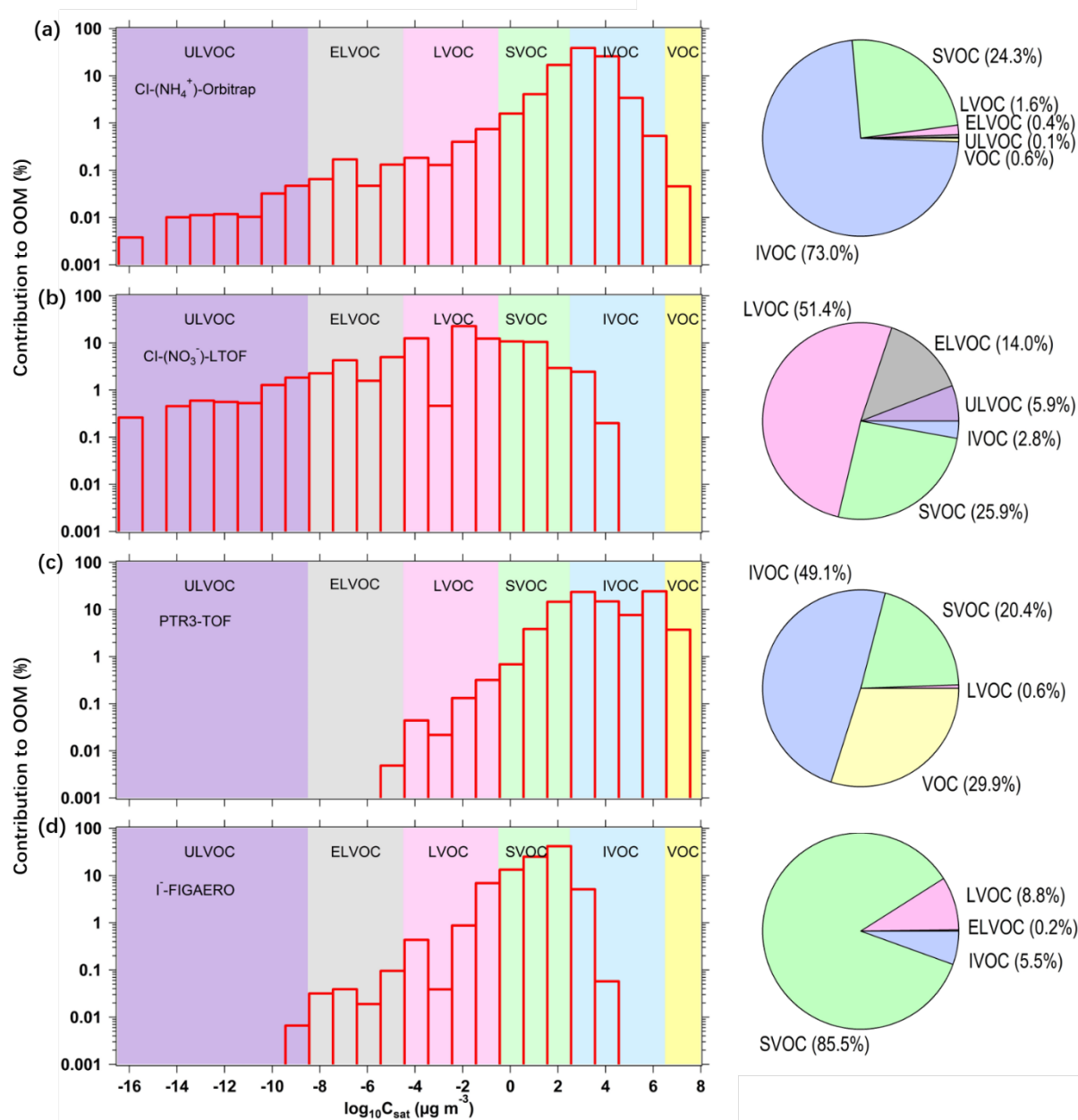
Figure 7: Volatility distribution comparison for organic compounds detected by (a) NH_4^+-Orbitrap, (b) NO_3^--LTOF, (c) PTR3-TOF and (d) I^--CIMS. The background colors represent the saturation concentration (C_{sat}) in the range of ultra-low volatility (ULVOCs, purple), extremely low volatility (ELVOCs, gray), low volatility (LVOCs, pink), semi-volatile (SVOCs, green), intermediate volatility (IVOCs, blue) and volatile organic compounds (VOCs). The right pie charts are the corresponding contributions of VOC, IVOC, SVOC, LVOC, ELVOC, and ULVOC classes in run 2211. Concentrations were used to calculate the contribution in each volatility bin for NO_3^--LTOF and PTR3-TOF, while signals were calculated for NH_4^+-Orbitrap and I^--CIMS.
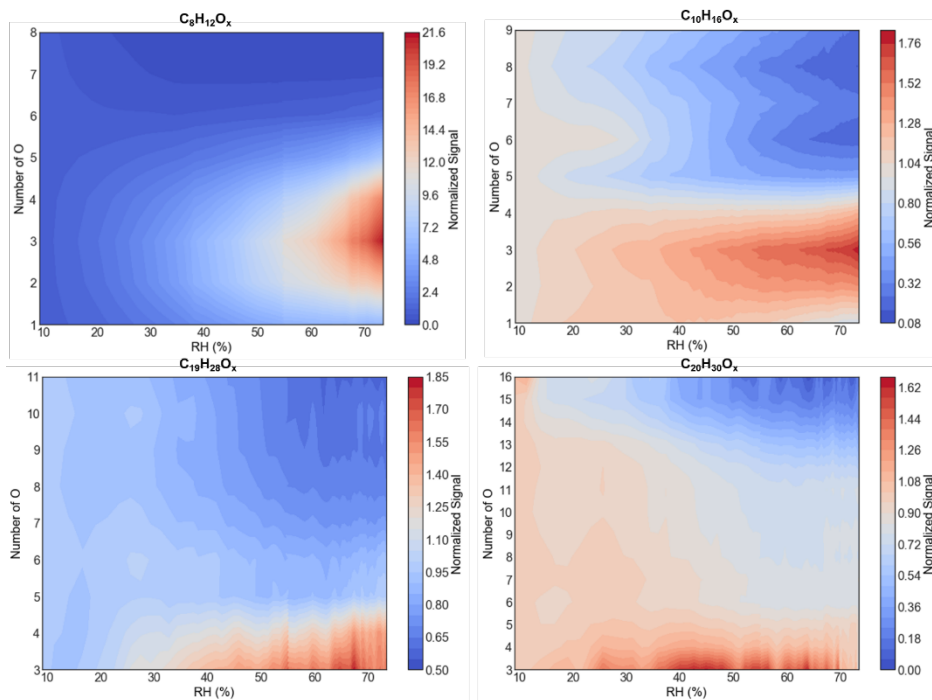
Figure 8: The effect of relative humidity on the distribution of the most abundant monomers and dimers measured by NH_4^+-Orbitrap. The RH ramped from ~10% to ~80% in run 2211. The normalized signal represents the signal variation ratio at certain RH compared to that at RH = 10%, normalized

$signal = \frac{signal_{RH}}{signal_{10\%}}$.